

Highly nonclassical phonon emission statistics through two-phonon loss of van der Pol oscillator

Jiahua Li,^{1,*} Chunling Ding,² and Ying Wu¹

¹*School of Physics, Huazhong University of Science and Technology, Wuhan 430074, People's Republic of China*

²*Hubei Key Laboratory of Optical Information and Pattern Recognition, Wuhan Institute of Technology, Wuhan 430205, People's Republic of China*

(Dated: August 25, 2020)

The ability to produce nonclassical wave in a system is essential for advances in quantum communication and computation. Here, we propose a scheme to generate highly nonclassical phonon emission statistics—antibunched wave in a quantum van der Pol (vdP) oscillator subject to an external driving, both single- and two-phonon losses. It is found that phonon antibunching depends significantly on the nonlinear two-phonon loss of the vdP oscillator, where the degree of the antibunching increases monotonically with the two-phonon loss and the distinguished parameter regimes with optimal antibunching and single-phonon emission are identified clearly. In addition, we give an in-depth insight into strong antibunching in the emitted phonon statistics by analytical calculations using a three-oscillator-level model, which agree well with the full numerical simulations employing both a master-equation approach and a Schrödinger-equation approach at weak driving. In turn, the fluorescence phonon emission spectra of the vdP oscillator, given by the power spectral density, are also evaluated. We further show that high phonon emission amplitudes, simultaneously accompanied by strong phonon antibunching, are attainable in the vdP system, which are beneficial to the correlation measurement in practical experiments. Our approach only requires a single vdP oscillator, without the need for reconfiguring the two coupled nonlinear resonators or the complex nanophotonic structures as compared to the previous unconventional blockade schemes. The present scheme could inspire methods to achieve antibunching in other systems.

PACS numbers: 42.60.Da, 42.50.Ct, 05.45.Xt, 42.65.-k

I. INTRODUCTION

Generating nonclassical antibunching light sources play an important role in many areas of research and applications [1–6]. Examples range from single-photon sources in emerging quantum technologies [7–12], single-photon transistors [13], single-photon quantum switching [14], single-photon quantum gates [15], photon turnstile [16] to quantum nonreciprocity [17]. Usually, there are two different approaches to realize strong photon antibunching (also called as photon blockade) through coherent quantum nonlinear systems [18].

One approach to efficiently create photon blockade is to require a very large nonlinear effect in quantum systems, which is referred to as conventional photon blockade [19–22]. The required optical nonlinearity can be typically induced by a strong interaction between the cavity mode and the dipole emitter (including, but not limited to, natural atom, small molecule, semiconductor quantum dot, and nitrogen vacancy center in diamond) or between the cavity mode and the mechanical mode, and so on, giving rise to an anharmonic energy-level ladder [23–25]. This kind of photon blockades have been theoretically and experimentally demonstrated in, for instance, cavity quantum electrodynamics [26–36], circuit quantum electrodynamics systems [37–39], waveguide quantum electrodynamics systems [40–44], cavity optome-

chanical systems [45–48], spinning or gain resonator systems [17, 49, 50], nanoplasmonic cavity-emitter systems [51–54], patterned two-dimensional material monolayer-cavity systems [55, 56], and other interesting systems [57–61].

The other approach to well achieve photon blockade is to exploit both a weak nonlinear effect and a quantum interference effect between various transition paths [62] or equivalently a displaced squeezed effect [63]. This approach, generally using two coupled cavities instead of one single cavity and thus without requiring strong nonlinear photon-photon interactions as compared to conventional photon blockade, is also named as unconventional photon blockade [62, 64]. Since then, numerous theoretical schemes based on such a physical mechanism without the constraint condition on the strong coupling have been proposed to obtain the strong antibunching, for example, in the bimodal cavity or two cavities coupling a quantum emitter [65–68], in the two directly coupled single-mode cavities with second-order or third-order optical nonlinearity [69–78], in the coupled cavity optomechanical systems [79–82], in the coupled polaritonic systems [83–85], and other special systems [86, 87]. Recently, this unconventional photon blockade has been observed experimentally by two groups based on two different setups, one using a two-level quantum dot embedded in a micropillar cavity with two orthogonally polarized modes [88] and the other using two coupled superconducting circuit resonators [89].

On the other hand, the van der Pol (vdP) oscillator is

* huajia_li@126.com

very extensive in natural and engineered systems. Since the prototypical model of the vdP oscillator was first proposed by Balthazar van der Pol in 1926 [90], it has attracted considerable attention in the classical level. In the past few years, this vdP model has been successfully extended from a classical regime to a quantum regime, i.e., the so-called quantum vdP oscillator, and also has drawn a great deal of research interests in the quantum level. The particles in vdP field are usually called the phonons based on the literatures [91–103]. We notice that the previous works shed light on the quantum synchronization, limit-cycle, frequency entrainment, and diverging and negative susceptibilities of a quantum vdP oscillator [91–99] or the entanglement tongue and quantum synchronization of two coupled quantum vdP oscillators [100–103], differing from what are found in the classical regime. To date, there seems to exist no works in the literature dealing with the above-mentioned nonclassical phonon antibunching in a quantum vdP oscillator. Is there strong antibunching effect? How does quantum noise (the dissipative coupling) effect the antibunching?

Motivated by these facts and to answer these issues above, in the present work we theoretically investigate the characteristics of antibunched phonons generated in a driven quantum vdP oscillator with both single- and two-phonon losses. By means of the second-order correlation function $g^{(2)}(0)$ providing information on phonon bunching and antibunching, we show that the degree of phonon antibunching is governed sensitively by the nonlinear two-phonon loss of the vdP oscillator. Increasing the two-phonon loss increases the degree of the phonon antibunching with experimentally achievable parameters. This occurs because a large two-photon loss decouples the third level of an oscillator leaving an effective driven two-level system. We identify clearly distinguished parameter regimes with strong antibunching and single-phonon emission. On the other hand, we present analytical solutions of the second-order correlation function based on a three-oscillator-level approximation, which match the full numerical simulations based on a quantum master equation and a Schrödinger equation at weak driving. Additionally, we analyze the fluorescence phonon emission spectra of the vdP oscillator by properly varying the two-phonon loss. It is found that high phonon emission amplitudes, accompanied by strong phonon antibunching (single-phonon emission), can be achieved efficiently. This result is useful for the correlation measurement in practical experiments.

Compared with the previous unconventional photon blockade schemes [62–68], our approach is based entirely on a single vdP oscillator, eliminating the need for coupled nonlinear resonators or complex nanophotonic structures. On the other hand, our achievable antibunching effect, $g^{(2)}(0) < 1$, can occur, without requiring fine trade-off and tuning between the loss rate and the nonlinearity. In particular, the degree of phonon antibunching can be kept high even for the case that the nonlinear two-phonon damping is less than the linear single-phonon damping.

Finally, we briefly discuss specific implementations based respectively on an ion trap [91–97] and an optomechanical membrane [104–106]. Our study contributes insights in understanding phonon-phonon correlation in the quantum vdP field.

This paper is organized as follows. In Sec. II, we describe the quantum model of a driven vdP oscillator under consideration and yield the Lindblad master equation which governs the dissipative dynamics of the vdP oscillator. In Sec. III, we introduce the second-order intensity correlation function which provides information on the degree of phonon bunching and antibunching. Subsequently, in Sec. IV, we provide analytical insights into the second-order correlation function based on a three-oscillator-level model (Sec. IV A) via a master equation approach and further find approximate solutions of the second-order correlation function (Sec. IV B). Again, starting from a Schrödinger equation approach, an analytical discussion for the second-order correlation function of the system is presented (Sec. IV C). This three-oscillator-level model is a justifiable approximation for low driving strengths. In Sec. V, we explore in details phonon correlation characteristics without and with time delay, as well as emission spectrum of the vdP oscillator by adjusting the typical parameters, especially dissipative engineering the two-phonon loss. In Sec. VI, we elaborate on an ion trap and optomechanical implementations of the quantum vdP oscillator. Finally, we summarize our results in Sec. VII.

II. SYSTEM OF A QUANTUM VDP OSCILLATOR: HAMILTONIAN AND MASTER EQUATION TREATMENT

We first introduce our model of the system. We consider a quantum vdP oscillator of interest, subject to an external continuous-wave driving of strength E_d and frequency ω_d , i.e., $S_{dri}(t) = E_d e^{-i\omega_d t}$. Our oscillator model involves two dissipation processes, one being a linear single-phonon loss of rate κ_1 and the other being a nonlinear two-phonon loss of rate κ_2 , as in Refs. [91–97]. Nevertheless, our model makes a slight adjustment of the usual quantum vdP oscillator, where the single-phonon gain is replaced with the single-phonon loss since the presence of the single-phonon loss is preferred to obtain strong phonon antibunching, and, on the other hand, it is much easier to achieve experimentally. Such dissipation processes can be engineered in current experimental platforms by coupling the oscillator to a suitable environment, as will be discussed later. The Hamiltonian and the Lindblad master equation for this model, in the frame rotating at the frequency ω_d of the external driving, read (setting $\hbar = 1$ throughout this work)

$$\hat{H}_{osc} = \hat{H}_0 + \hat{H}_{dri} = \Delta \hat{a}^\dagger \hat{a} + i E_d (\hat{a} - \hat{a}^\dagger), \quad (1)$$

$$\frac{d\hat{\rho}}{dt} = -i[\hat{H}_{osc}, \hat{\rho}] + \frac{1}{2}\kappa_1 \mathcal{D}(\hat{a})\hat{\rho} + \frac{1}{2}\kappa_2 \mathcal{D}(\hat{a}^2)\hat{\rho}, \quad (2)$$

where \hat{a} (\hat{a}^\dagger) is the oscillator annihilation (creation) operator satisfying bosonic commutation relation $[\hat{a}, \hat{a}^\dagger] = 1$, $\Delta = \omega_a - \omega_d$ is the detuning between the vdP oscillator frequency ω_a and the external driving frequency ω_d , and $\hat{\rho}$ is the density matrix operator, respectively. Applying the unitary transformation $\hat{U} = \exp(i\omega_d \hat{a}^\dagger \hat{a} t)$ leads to Eq. (1) above: $\hat{H}_{osc} = \hat{U} \hat{H}_{old} \hat{U}^\dagger - i\hat{U} \partial \hat{U}^\dagger / \partial t$, where $\hat{H}_{old} = \omega_a \hat{a}^\dagger \hat{a} + iE_d (e^{i\omega_d t} \hat{a} - e^{-i\omega_d t} \hat{a}^\dagger)$, under the helps of $\hat{U} \hat{a} \hat{U}^\dagger = \hat{a} e^{-i\omega_d t}$, $\hat{U} \hat{a}^\dagger \hat{U}^\dagger = \hat{a}^\dagger e^{i\omega_d t}$, and $\hat{U} \partial \hat{U}^\dagger / \partial t = -i\omega_d \hat{a}^\dagger \hat{a}$. In the driving term $\hat{H}_{driv} = iE_d (\hat{a} - \hat{a}^\dagger)$ in Eq. (1), the rotating-wave approximation has been applied; without the loss of generality, we set E_d to be real. $\hat{H}_0 = \Delta \hat{a}^\dagger \hat{a}$ is the unperturbed Hamiltonian of the oscillator relative to ω_d . Above, in Eq. (2) we have introduced the Lindblad operator $\mathcal{D}(\hat{O})\hat{\rho} = 2\hat{O}\hat{\rho}\hat{O}^\dagger - \hat{\rho}\hat{O}^\dagger\hat{O} - \hat{O}^\dagger\hat{O}\hat{\rho}$ to describe the nonunitary dynamics with \hat{O} being the relevant operators \hat{a} and \hat{a}^2 . This master equation can be used to derive the steady state for the following second-order correlation function.

III. SECOND-ORDER CORRELATION FUNCTION PROVIDING INFORMATION ON PHONON (ANTI)BUNCHING

The appeal of the quantum vdP oscillator is that owing to its simple form, it can serve as a prototypical model for studying its nonclassical properties in the quantum limit. Here we concentrate on the phonon statistics of the quantum vdP oscillator. To this end, our central task in this work is to calculate the normalized second-order correlation function $g^{(2)}(\tau)$, which is defined, for the vdP oscillator in the steady state, as [107–110]

$$\begin{aligned} g^{(2)}(\tau) &= \frac{\text{Tr}[\hat{\rho} \hat{a}^\dagger(0) \hat{a}^\dagger(\tau) \hat{a}(\tau) \hat{a}(0)]}{\{\text{Tr}[\hat{\rho} \hat{a}^\dagger(0) \hat{a}(0)]\}^2} \\ &= \frac{\langle \hat{a}^\dagger(0) \hat{a}^\dagger(\tau) \hat{a}(\tau) \hat{a}(0) \rangle}{\langle \hat{a}^\dagger(0) \hat{a}(0) \rangle^2}, \end{aligned} \quad (3)$$

where $\langle \hat{O} \rangle = \text{Tr}(\hat{\rho} \hat{O})$ denotes the expectation values taken with respect to the steady-state density matrix of the full Lindblad master equation (2), and τ is the time between the arrival of the first and second phonons, i.e., time delay. $g^{(2)}(\tau)$ can be understood as the conditional probability of detecting a phonon at time τ provided that one phonon was detected earlier at time $\tau = 0$. It can be proved that the second-order correlation function $g^{(2)}(\tau)$ satisfies the properties of, on the one hand, time symmetry $g^{(2)}(-\tau) = g^{(2)}(\tau)$, and, on the other hand, non-negativity $g^{(2)}(\tau) \geq 0$.

If $\tau = 0$, we refer to $g^{(2)}(0)$ as a zero-time-delay second-order correlation function. For the case of zero time delay, it is known that the value of $g^{(2)}(0) < 1$ [$g^{(2)}(0) > 1$] corresponds to sub-Poissonian (super-Poissonian) statistics of the vdP oscillator field, which is a nonclassical antibunching (classical bunching) effect. Alternatively, $g^{(2)}(0) = 1$ represents a coherent light source.

One can numerically calculate the steady-state solution of the master equation Eq. (2) with the left-hand side set to zero, from which the steady-state second-order correlation function $g^{(2)}(\tau)$ is obtained. For this purpose, we truncate the vdP field's Hilbert space sufficiently large, for example, at phonon numbers as large as 100 for the vdP oscillator mode to ensure full convergence. Finally, all calculations are performed in the frame rotating with the driving frequency ω_d .

IV. TWO-TYPE ANALYTICAL INSIGHTS INTO THE SECOND-ORDER CORRELATION FUNCTION BY A THREE-OSCILLATOR-LEVEL APPROXIMATION

A. Three-oscillator-level approximation via a master equation approach

Before proceeding, we develop a three-oscillator-level model that provides further physical insight into the numerical results. For this purpose, in the Hilbert space of Fock states $\{|n\rangle\}$ with $n = 0, 1, 2, \dots$ being the number of phonons in the oscillator mode, the Lindblad master equation (2) can be written as

$$\begin{aligned} \frac{d\rho_{n,m}}{dt} &= -i\Delta(n-m)\rho_{n,m} \\ &+ E_d(\sqrt{n+1}\rho_{n+1,m} - \sqrt{n}\rho_{n-1,m}) \\ &+ E_d(\sqrt{m+1}\rho_{n,m+1} - \sqrt{m}\rho_{n,m-1}) \\ &+ \kappa_1 \left[\sqrt{(n+1)(m+1)}\rho_{n+1,m+1} - \frac{n+m}{2}\rho_{n,m} \right] \\ &+ \kappa_2 \left[\sqrt{(n+1)(n+2)}\sqrt{(m+1)(m+2)}\rho_{n+2,m+2} \right. \\ &\quad \left. - \frac{n(n-1) + m(m-1)}{2}\rho_{n,m} \right], \end{aligned} \quad (4)$$

where $\rho_{n,m} = \langle n | \hat{\rho} | m \rangle = \langle m | \hat{\rho} | n \rangle^*$ is the matrix element of the density operator $\hat{\rho}$. The diagonal element $\rho_{n,n}$ denotes the occupying probability in the state $|n\rangle$, whereas the off-diagonal element $\rho_{n,m}$ ($n \neq m$) represents the coherence between the states $|n\rangle$ and $|m\rangle$.

Next, we approximate the oscillator modes by retaining the lowest three oscillator levels, $n = 0, 1, 2$, in Eq. (4). In this scenario, we have the equations of motion for the density operator matrix element $\rho_{n,m}$ as follows:

$$\begin{aligned} \frac{d\rho_{1,1}}{dt} &= -\kappa_1\rho_{1,1} + 2\kappa_1\rho_{2,2} + \sqrt{2}E_d\rho_{2,1} + \sqrt{2}E_d\rho_{1,2} \\ &\quad - E_d\rho_{0,1} - E_d\rho_{1,0}, \end{aligned} \quad (5)$$

$$\frac{d\rho_{2,2}}{dt} = -2(\kappa_1 + \kappa_2)\rho_{2,2} - \sqrt{2}E_d\rho_{2,1} - \sqrt{2}E_d\rho_{1,2}, \quad (6)$$

$$\begin{aligned} \frac{d\rho_{1,0}}{dt} &= -\left(i\Delta + \frac{1}{2}\kappa_1\right)\rho_{1,0} + 2E_d\rho_{1,1} + E_d\rho_{2,2} \\ &\quad + \sqrt{2}\kappa_1\rho_{2,1} + \sqrt{2}E_d\rho_{2,0} - E_d, \end{aligned} \quad (7)$$

$$\frac{d\rho_{2,1}}{dt} = -\left(i\Delta + \frac{3}{2}\kappa_1 + \kappa_2\right)\rho_{2,1} + \sqrt{2}E_d(\rho_{2,2} - \rho_{1,1})$$

$$-E_d\rho_{2,0}, \quad (8)$$

$$\frac{d\rho_{2,0}}{dt} = -(2i\Delta + \kappa_1 + \kappa_2)\rho_{2,0} + E_d\rho_{2,1} - \sqrt{2}E_d\rho_{1,0}, \quad (9)$$

where $\rho_{0,0} = 1 - \rho_{1,1} - \rho_{2,2}$.

In the steady state limit, i.e., setting $d\rho_{n,m}/dt = 0$ in the left-hand side of Eqs. (5)-(9), we have the results

$$-\kappa_1\rho_{1,1} + 2\kappa_1\rho_{2,2} + \sqrt{2}E_d\rho_{2,1} + \sqrt{2}E_d\rho_{1,2} - E_d\rho_{0,1} - E_d\rho_{1,0} = 0, \quad (10)$$

$$-2(\kappa_1 + \kappa_2)\rho_{2,2} - \sqrt{2}E_d\rho_{2,1} - \sqrt{2}E_d\rho_{1,2} = 0, \quad (11)$$

$$-\left(i\Delta + \frac{1}{2}\kappa_1\right)\rho_{1,0} + 2E_d\rho_{1,1} + E_d\rho_{2,2} + \sqrt{2}\kappa_1\rho_{2,1}$$

$$+\sqrt{2}E_d\rho_{2,0} = E_d, \quad (12)$$

$$-\left(i\Delta + \frac{3}{2}\kappa_1 + \kappa_2\right)\rho_{2,1} + \sqrt{2}E_d(\rho_{2,2} - \rho_{1,1}) - E_d\rho_{2,0} = 0, \quad (13)$$

$$-(2i\Delta + \kappa_1 + \kappa_2)\rho_{2,0} + E_d\rho_{2,1} - \sqrt{2}E_d\rho_{1,0} = 0. \quad (14)$$

This set of equations (10)-(14) together with the corresponding complex conjugations can be solved by first expressing in the matrix form,

$$\mathbf{MR} = \mathbf{V}, \quad (15)$$

where the elements of the matrices are respectively presented by $\mathbf{R} = (\rho_{1,1}, \rho_{2,2}, \rho_{1,0}, \rho_{0,1}, \rho_{2,1}, \rho_{1,2}, \rho_{2,0}, \rho_{0,2})^T$, $\mathbf{V} = (0, 0, E_d, E_d, 0, 0, 0, 0)^T$, and

$$\mathbf{M} = \begin{pmatrix} -\kappa_1 & 2\kappa_2 & -E_d & -E_d & \sqrt{2}E_d & \sqrt{2}E_d & 0 & 0 \\ 0 & -2(\kappa_1 + \kappa_2) & 0 & 0 & -\sqrt{2}E_d & -\sqrt{2}E_d & 0 & 0 \\ 2E_d & E_d & -i\Delta - \frac{1}{2}\kappa_1 & 0 & \sqrt{2}\kappa_1 & 0 & \sqrt{2}E_d & 0 \\ 2E_d & E_d & 0 & i\Delta - \frac{1}{2}\kappa_1 & 0 & \sqrt{2}\kappa_1 & 0 & \sqrt{2}E_d \\ -\sqrt{2}E_d & \sqrt{2}E_d & 0 & 0 & -i\Delta - \frac{3}{2}\kappa_1 - \kappa_2 & 0 & -E_d & 0 \\ -\sqrt{2}E_d & \sqrt{2}E_d & 0 & 0 & 0 & i\Delta - \frac{3}{2}\kappa_1 - \kappa_2 & 0 & -E_d \\ 0 & 0 & -\sqrt{2}E_d & 0 & E_d & 0 & -2i\Delta - \kappa_1 - \kappa_2 & 0 \\ 0 & 0 & 0 & -\sqrt{2}E_d & 0 & E_d & 0 & 2i\Delta - \kappa_1 - \kappa_2 \end{pmatrix}.$$

The solutions of \mathbf{R} are given by $\mathbf{R} = \mathbf{M}^{-1}\mathbf{V}$ with \mathbf{M}^{-1} denoting the inverse matrix of \mathbf{M} , and here \mathbf{M}^{-1} is too lengthy and uninspiring to be displayed. In order to capture the main physics, we consider some particular cases of interest and derive closed-form expressions of \mathbf{R} . First, the driving is set on resonance with the vdP oscillator, i.e., $\Delta = 0$ for simplicity. Second, the condition of

weak external driving holds, i.e., $E_d \ll \kappa_1, \kappa_2$, in order to guarantee the validity of the three-level model. With these assumptions discussed above, $\rho_{1,1}$ and $\rho_{2,2}$ we need in the solutions of \mathbf{R} [see Eq. (20) later for clarity], to the quartic order in the variables E_d/κ_1 and E_d/κ_2 after tedious calculations, are

$$\rho_{1,1} = \left[2 + \frac{\kappa_1^2}{4E_d^2} + \frac{2\kappa_1\kappa_2 - 2\kappa_1^2}{(\kappa_1 + \kappa_2)(3\kappa_1 + 2\kappa_2)} - \frac{4\kappa_1}{3\kappa_1 + 2\kappa_2} + \frac{\kappa_1}{\kappa_1 + \kappa_2} + \frac{8\kappa_2E_d^2}{(\kappa_1 + \kappa_2)^2(3\kappa_1 + 2\kappa_2)} \right]^{-1}, \quad (16)$$

$$\rho_{2,2} = \left[\frac{4E_d^2}{(\kappa_1 + \kappa_2)(3\kappa_1 + 2\kappa_2)} + \frac{2\kappa_1E_d^2}{(\kappa_1 + \kappa_2)^2(3\kappa_1 + 2\kappa_2)} \right] \rho_{1,1}. \quad (17)$$

B. Analytical expressions for the second-order correlation function

According to $\hat{a}^\dagger \hat{a}|n\rangle = n|n\rangle$ and $\hat{a}^{\dagger 2} \hat{a}^2|n\rangle = n(n-1)|n\rangle$, we have $\langle n|\hat{\rho} \hat{a}^\dagger \hat{a}|n\rangle = n\rho_{n,n}$ and $\langle n|\hat{\rho} \hat{a}^{\dagger 2} \hat{a}^2|n\rangle = n(n-1)\rho_{n,n}$. So, the zero-time-delay second-order correlation function $g^{(2)}(0)$ can be recast in the form

$$g^{(2)}(0) = \frac{\sum_n n(n-1)\rho_{n,n}}{\left(\sum_n n\rho_{n,n}\right)^2}$$

$$= \frac{2\rho_{2,2} + 6\rho_{3,3} + \dots}{(\rho_{1,1} + 2\rho_{2,2} + \dots)^2}, \quad (18)$$

where the sum index $n = 0, 1, 2, \dots$. Obviously, non-classical antibunching (sub-Poissonian statistics) requires that the numerator of Eq. (18) is smaller than its denominator. For example, this can be achieved either by maximizing $\rho_{1,1}$ or decreasing $\rho_{2,2}$. Note that, the component of $n = 0$ need not be considered owing to the vanishing value.

Under the weak driving condition where $\rho_{n,n}$ vanishes

quickly with n , we have the relationship

$$\rho_{0,0} \gg \rho_{1,1} \gg \rho_{2,2} \gg \rho_{3,3} \gg \dots \quad (19)$$

In view of this, by the truncation, the $g^{(2)}(0)$ function from Eq. (18) can be approximately reduced into the simple expression

$$g^{(2)}(0) \simeq \frac{2\rho_{2,2}}{\rho_{1,1}^2}, \quad (20)$$

or

$$g^{(2)}(0) \simeq \left[\frac{8E_d^2}{(\kappa_1 + \kappa_2)(3\kappa_1 + 2\kappa_2)} + \frac{4\kappa_1 E_d^2}{(\kappa_1 + \kappa_2)^2(3\kappa_1 + 2\kappa_2)} \right] \times \frac{1}{\rho_{1,1}}, \quad (21)$$

where the two desired matrix elements $\rho_{2,2}$ and $\rho_{1,1}$ are yielded by Eqs. (16) and (17).

As an aside, we note that when the two-phonon loss is much stronger than the single-phonon loss ($\kappa_2 \gg \kappa_1$), retaining the lowest order in E_d/κ_1 , E_d/κ_2 and κ_1/κ_2 , the $g^{(2)}(0)$ function from Eq. (21) can be further reduced into a compact form

$$g^{(2)}(0) \simeq \left(\frac{\kappa_1}{\kappa_2} \right)^2 \sim 0, \quad (22)$$

which coincides with the numerical simulation based on the full quantum master equation (2) in the aforementioned parameter range, as can be found in Fig. 1 below.

C. Three-oscillator-level approximation via a Schrödinger equation approach

From another point of view, now we consider the Schrödinger equation approach to analytically calculate the second-order correlation function. Likewise, under the condition that the external driving laser field is very weak (i.e., $E_d \ll \kappa_1, \kappa_2$), the aforementioned excitation number n of the vdP oscillator is no more than two (i.e., $n \leq 2$ corresponding to the so-called three-oscillator-level truncation). In this scenario, the quantum state of the vdP oscillator system can be written as

$$|\psi\rangle = c_0|0\rangle + c_1|1\rangle + c_2|2\rangle, \quad (23)$$

where the coefficient c_n represents the amplitude of the corresponding quantum state $|n\rangle$ ($n = 0, 1, 2$).

In order to achieve the coefficient c_n above, we need to solve the following Schrödinger equation

$$i \frac{\partial |\psi\rangle}{\partial t} = \hat{H}_{osc} |\psi\rangle, \quad (24)$$

where \hat{H}_{osc} is the modified non-Hermitian Hamiltonian of the system including phenomenologically both the linear single-phonon loss (κ_1) and nonlinear two-phonon loss (κ_2) terms, with the form

$$\hat{H}_{osc} = -i \frac{1}{2} \kappa_1 \hat{a}^\dagger \hat{a} - i \frac{1}{2} \kappa_2 \hat{a}^{\dagger 2} \hat{a}^2 + \Delta \hat{a}^\dagger \hat{a} + i E_d (\hat{a} - \hat{a}^\dagger). \quad (25)$$

According to Eq. (24), we can directly obtain a set of coupled algebraic equations about the coefficient c_n as follows

$$\frac{\partial c_0}{\partial t} = E_d c_1, \quad (26)$$

$$\frac{\partial c_1}{\partial t} = -i \Delta c_1 - \frac{1}{2} \kappa_1 c_1 - E_d c_0 + \sqrt{2} E_d c_2, \quad (27)$$

$$\frac{\partial c_2}{\partial t} = -2i \Delta c_2 - \kappa_1 c_2 - \kappa_2 c_2 - \sqrt{2} E_d c_1. \quad (28)$$

In the limit of the above-mentioned weak-driving, we can take $c_0 \simeq 1$ [thus Eq. (26) can be dropped] and neglect the third-order term $\sqrt{2} E_d c_2$ (we only retain the terms up to the second order) in Eq. (27). Under the steady-state situation, $\partial |c_n\rangle / \partial t = 0$, we have the results

$$-i \Delta c_1 - \frac{1}{2} \kappa_1 c_1 - E_d = 0, \quad (29)$$

$$-2i \Delta c_2 - \kappa_1 c_2 - \kappa_2 c_2 - \sqrt{2} E_d c_1 = 0. \quad (30)$$

After some straightforward calculations, the solutions to Eqs. (29) and (30) for the coefficients c_1 and c_2 are found to be

$$c_1 = -\frac{2E_d}{2i\Delta + \kappa_1}, \quad (31)$$

$$c_2 = -\frac{\sqrt{2}E_d c_1}{2i\Delta + \kappa_1 + \kappa_2}, \quad (32)$$

which are closely related to the matrix elements $\rho_{1,1}$ and $\rho_{2,2}$ via the relationships $\rho_{1,1} = |c_1|^2$ and $\rho_{2,2} = |c_2|^2$. So, based on Eq. (20), we can derive a closed-form expression for the $g^{(2)}(0)$ function as

$$g^{(2)}(0) \simeq \frac{\kappa_1^2 + 4\Delta^2}{(\kappa_1 + \kappa_2)^2 + 4\Delta^2}, \quad (33)$$

where for the significantly large detuning Δ , $g^{(2)}(0)$ approaches the value of 1. For the resonance driving $\Delta = 0$, the $g^{(2)}(0)$ function is further simplified to $g^{(2)}(0) \simeq \kappa_1^2 / (\kappa_1 + \kappa_2)^2$. In this scenario of $\Delta = 0$, for large κ_2 , $g^{(2)}(0)$ tends to the value of 0, while for small κ_2 , $g^{(2)}(0)$ tends to the value of 1. These results are in good agreement with the numerical simulations based on the full quantum master equation (2) in Figs. 1(a) and 1(b) later.

Physically, the zero value of $g^{(2)}(0)$ can be understood from the κ_2/κ_1 ratio determining the structure of the discrete energy level in the quantum circumstance: the quantum vdP oscillator is favorable to be restricted to the lowest Fock states as the nonlinear two-phonon loss κ_2 increases, which has been pointed out in Refs. [100, 101]. In the limit of $\kappa_2 \gg \kappa_1$, only the two lowest Fock states $|0\rangle$ and $|1\rangle$ are occupied. In this quantum regime, the nonlinearity of the dissipation prevents reaching the two phonon state, that is to say, the transition pathway from Fock states $|1\rangle$ to $|2\rangle$ is virtually forbidden, so realizing phonon blockade is possible.

Finally, it is worth pointing out that, via comparing the two-type treatments [(i) the master equation approach and (ii) the Schrödinger equation approach], it is clearly

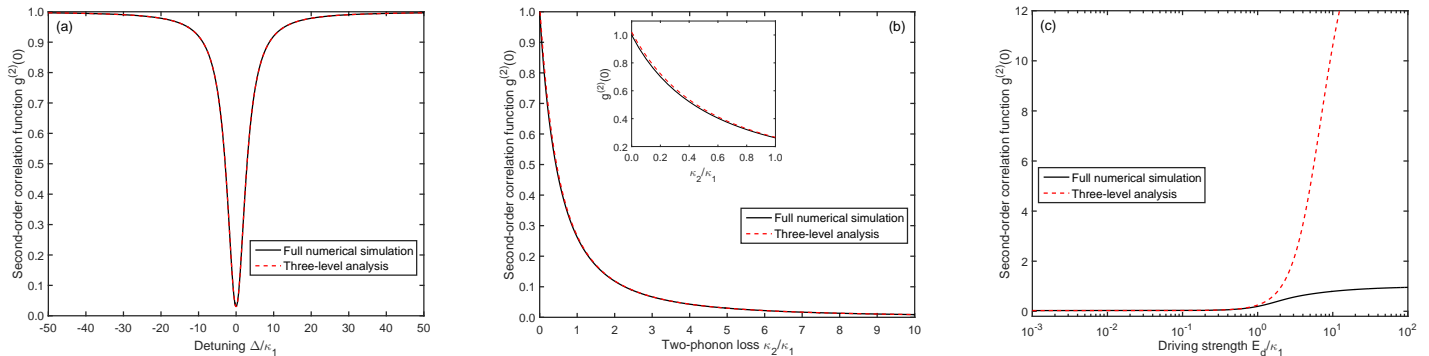


FIG. 1. (a) Zero-delay second-order correlation function $g^{(2)}(0)$ of the vdP oscillator plotted as a function of the dimensionless detuning Δ/κ_1 for the two-photon loss rate $\kappa_2/\kappa_1 = 5$ and the driving strength $E_d/\kappa_1 = 0.1$. (b) Dependence of zero-delay second-order correlation function $g^{(2)}(0)$ on the dimensionless two-photon loss rate κ_2/κ_1 , plotted for the zero detuning $\Delta/\kappa_1 = 0$ and the driving strength $E_d/\kappa_1 = 0.1$. The inset shows a zoom-in view of the $\kappa_2 < \kappa_1$ region. (c) Dependence of zero-delay second-order correlation function $g^{(2)}(0)$ on the dimensionless driving strength E_d/κ_1 for changing logarithmically from 0.001 to 100, plotted for the zero detuning $\Delta/\kappa_1 = 0$ and the two-photon loss rate $\kappa_2/\kappa_1 = 5$. In panels (a)-(c), the black solid lines denote full numerical simulations of a quantum master equation from Eq. (2), whereas the red dashed lines are analytical calculations of a three-oscillator-level model from Eq. (15).

shown that the Schrödinger equation approach is more robust and straightforward. Nevertheless, its deficiency is that the dissipations of the system are phenomenologically added.

V. RESULT ANALYSES AND DISCUSSIONS

Figure 1 shows the steady-state value of the normalized second-order correlation function at zero-time delay, $g^{(2)}(0)$, as a function of the detuning δ [panel (a)], the two-photon loss κ_2 [panel (b)], and the driving strength E_d [panel (c)], respectively. All plotted parameters are in units of the single-phonon loss κ_1 and thus are dimensionless. The black solid lines represent full numerical simulations from the quantum master equation (1), while the red dashed lines are analytical calculations predicted by Eq. (15) from the three-oscillator-level approximation. To be specific, it can be seen from Fig. 1(a) that the profile of the second-order correlation function $g^{(2)}(0)$ is symmetric with respect to the detuning Δ . There is a marked antibunching dip at $\Delta = 0$, corresponding to a minimum value of $g^{(2)}(0) \simeq 0.03$ in good agreement with Eq. (33). Increasing $|\Delta|$ leads to an increase in $g^{(2)}(0)$, degrading the degree of antibunching. For significantly large $|\Delta|$, $g^{(2)}(0)$ approaches a saturation value of unity, indicating coherent light emission. Numerical simulations matching analytical calculations show that the strong phonon antibunching can be achieved by utilizing the typical parameter values, e.g., $\kappa_2 = 5\kappa_1$ and $E_d = 0.1\kappa_1$ given in Fig. 1(a), not specific values from any one experiment. In order to understand the physics behind this antibunching effect, intuitively, we look at the role of the κ_2 parameter, as will be discussed later.

As illustrated in Fig. 1(b), when the two-photon loss

κ_2 is set to zero, $g^{(2)}(0)$ is equal to 1, suggesting coherent light emitted from the vdP oscillator. Again, we can clearly see that $g^{(2)}(0)$ monotonically and rapidly decreases from 1 as κ_2 increases, asymptotically approaching zero for large κ_2 . For $\kappa_2 \sim 0.4\kappa_1$, $g^{(2)}(0)$ can reach 0.5. The value $g^{(2)}(0) < 0.5$ is considered as an upper bound for single-phonon emission [43, 74, 78, 111]. As a consequence, the criterion for single-phonon emission can hold when $\kappa_2 > 0.4\kappa_1$. Such dissipative processes can be engineered in current experimental devices [91, 92, 112], as will be illustrated in Sec. VI below. Note that, in Fig. 1(b), we keep the parameters $\Delta = 0$ and $E_d = 0.1\kappa_1$ fixed. In this scenario, the analytical $g^{(2)}(0)$ [black solid line in Fig. 1(b)] agrees very well with the numerically exact results [red dashed line in Fig. 1(b)]. Overall, the two-photon loss dependence of phonon emission statistics shows that the degree of phonon antibunching can be kept high even for $\kappa_2 < \kappa_1$.

In light of the above analyses from Figs. 1(a) and (b), we can conclude that the validity of such a three-oscillator-level approximation is not dependent on both the Δ and κ_2 parameters. What is the breakdown of this three-oscillator-level approximation? To help answer this question, in Fig. 1(c) we displays a typical case for varying the driving strength E_d while keeping $\Delta = 0$ and $\kappa_2 = 5\kappa_1$ fixed. Looking closer, we see that for small driving strengths in the range $E_d \leq \kappa_1$, this three-level analysis closely matches the result of the master equation simulation shown in Fig. 1(c). However, when the ratio E_d/κ_1 is larger than 1, the three-level approximation completely fails to account for $g^{(2)}(0)$. With this fact, we notice from the black solid line of Fig. 1(c) that, as E_d increases logarithmically from 0.001 to 100, $g^{(2)}(0)$ grows from a constant value close to zero, corresponding to single-phonon emission ($E_d \leq \kappa_1$), to an unity saturation value indi-

ating coherent light emission ($E_d > 80\kappa_1$). It is worth pointing out that strong antibunching [$g^{(2)}(0) \sim 0$] features a long plateau about E_d .

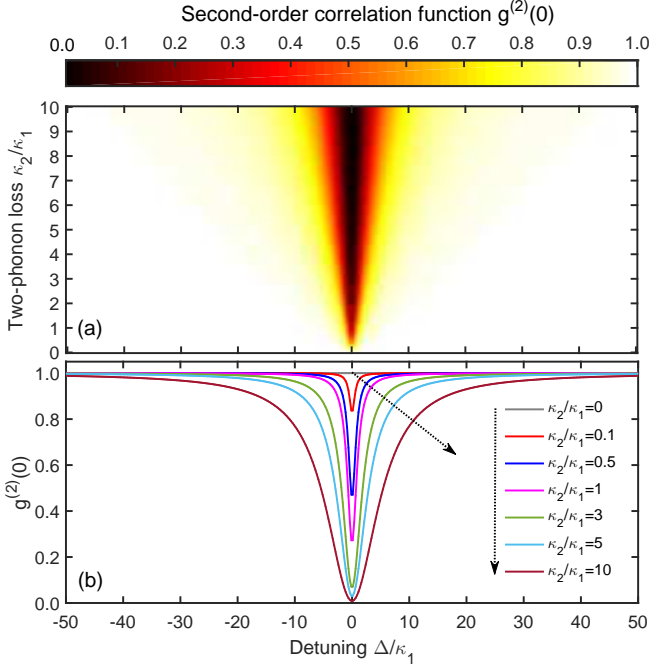


FIG. 2. (a) 2D contour plot of zero-delay second-order correlation function $g^{(2)}(0)$ versus the detuning Δ/κ_1 and the two-phonon loss rate κ_2/κ_1 for the driving strength $E_d/\kappa_1 = 0.1$. (b) Cross section of (a) along the Δ axis, for seven fixed sets of the two-phonon loss rate $\kappa_2/\kappa_1 = 0, 0.1, 0.5, 1, 3, 5,$ and 10 .

To gain further insight, Figure 2(a) displays the color-scale maps of the normalized second-order correlation function $g^{(2)}(0)$ as a function of both the detuning Δ and the two-phonon loss κ_2 . Figure 2(b) shows the cuts through the horizontal Δ -axis for seven different values of κ_2 . It follows that the antibunching window width increases with increasing κ_2 . Moreover, the degree of the antibunching is more pronounced as κ_2 is increased, whether the applied driving is set on resonance with the vdP oscillator or not. A natural question is, then, why the dissipation κ_2 plays an important role in generating phonon antibunching? As it is well known, the phonon dissipation offers a major source of decoherence [107–110], giving rise to the expectation that the dissipation should always weaken the antibunching. Physically, this is mainly because the two terms ($\frac{1}{2}\kappa_2 a^{\dagger 2} a^{\dagger 2} \rho$ and $\frac{1}{2}\kappa_2 \rho a^{\dagger 2} a^{\dagger 2}$) in the two-phonon dissipation expression of Eq. (1) act as the Kerr nonlinearity $\chi^{(3)}$ (see, for instance, Refs. [97–99], and references therein). As an example, the dynamical evolution equations of the key field operator in the respective system are analogous; specifically, one is $\partial \hat{a} / \partial t = -i\Delta \hat{a} - \frac{1}{2}\kappa_1 \hat{a} - \kappa_2 \hat{a}^\dagger \hat{a} \hat{a} - E_d$ for the vdP oscillator, the other is $\partial \hat{a} / \partial t = -i\Delta \hat{a} - \frac{1}{2}\kappa_1 \hat{a} - i\chi^{(3)} \hat{a}^\dagger \hat{a} \hat{a} - E_d$ for the Kerr nonlinear resonator. However, the present vdP

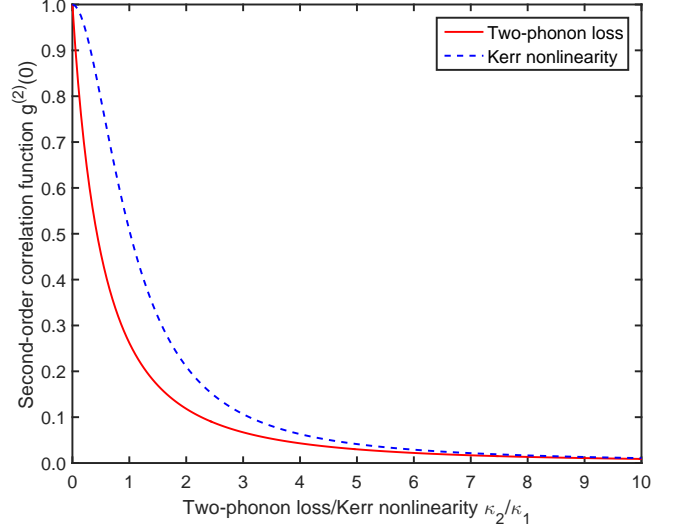


FIG. 3. Comparison of the normalized second-order correlation function $g^{(2)}(0)$ obtained via the two-phonon loss in the vdP oscillator to that obtained via the Kerr nonlinearity in the resonator which only includes a single-phonon loss. Here the resulting effective Hamiltonian and the Lindblad master equation of the Kerr nonlinear resonator, respectively, are yielded by $\hat{H}_{KN} = \Delta \hat{a}^\dagger \hat{a} + \frac{1}{2}\kappa_2 \hat{a}^{\dagger 2} \hat{a}^2 + iE_d(\hat{a} - \hat{a}^\dagger)$ and $d\hat{\rho}/dt = -i[\hat{H}_{KN}, \hat{\rho}] + \kappa_1 D(\hat{a})\hat{\rho}$ in a rotating frame with respect to $\hat{H}_0 = \omega_d \hat{a}^\dagger \hat{a}$. See main text about the vdP oscillator for more details. The other system parameters are set as $E_d/\kappa_1 = 0.1$ and $\Delta/\kappa_1 = 0$.

oscillator for realizing the antibunching outperforms the Kerr nonlinear resonator when setting $\chi^{(3)} = \kappa_2$ and the other common parameters are the same as in Fig. 1(a), as verified from Fig. 3. A striking feature of the results of Fig. 3 is the fact that, for an identical κ_2 , the degree of the phonon antibunching for the vdP oscillator is much smaller than that for the Kerr nonlinear resonator. Thus, the antibunching phenomenon is more pronounced relative to the Kerr nonlinear resonator.

In the following, we elaborate on the amount of phonon emission through the vdP oscillator corresponding to the driving used in Figs. 1(a) and (b), as we collect the fluorescence primarily from the oscillator. These would be of interest in designing a practical experiment, as it would be of consequence to the number of counts that are obtained in the correlation measurement. To this end, the fluorescence phonon emission spectrum of the vdP oscillator is yielded by the power spectral density (PSD), which is defined as the Fourier transform of the first-order correlation function of the vdP oscillator field, namely, $S(\omega) = \int_{-\infty}^{\infty} \langle \hat{a}^\dagger(\tau) \hat{a}(0) \rangle e^{-i(\omega - \omega_d)\tau} d\tau$ [107–109], where the angular brackets represent the average in the steady state of Eq. (2) and the calculation is performed in the frame rotating with the driving frequency ω_d . The PSD of the vdP mode can be directly monitored in experiments.

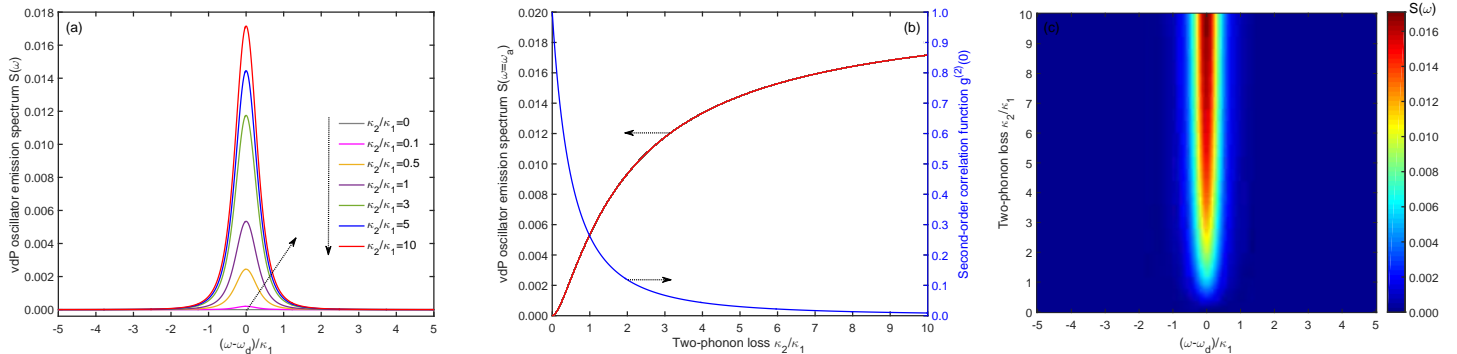


FIG. 4. (a) Phonon emission spectrum $S(\omega)$, i.e., PSD as a function of the dimensionless frequency $(\omega - \omega_d)/\kappa_1$ for a resonantly driven vdP oscillator in a frame rotating at the driving frequency ω_d . The other system parameters are chosen as $E_d/\kappa_1 = 0.1$ and $\Delta/\kappa_1 = 0$, respectively. (b) Value of the spectrum $S(\omega = \omega_a)$ at the vdP oscillator frequency ω_a as a function of the two-photon loss rate κ_2/κ_1 on the left-hand axis. Zero-delay second-order correlation function $g^{(2)}(0)$ as a function of the two-photon loss rate κ_2/κ_1 on the right-hand axis. The other system parameters are set as $E_d/\kappa_1 = 0.1$ and $\Delta/\kappa_1 = 0$. (c) 2D contour plot of vdP oscillator emission spectrum $S(\omega)$ versus the frequency $(\omega - \omega_d)/\kappa_1$ and the two-photon loss rate κ_2/κ_1 for $E_d/\kappa_1 = 0.1$ and $\Delta/\kappa_1 = 0$.

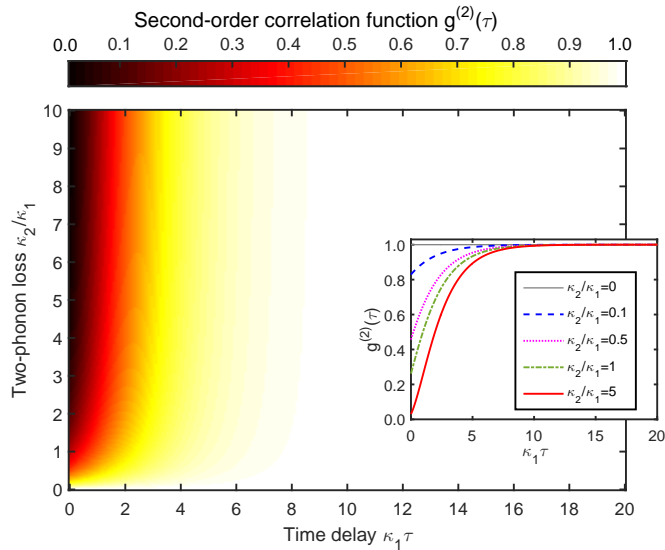


FIG. 5. 2D contour plot of delayed second-order correlation function $g^{(2)}(\tau)$ as a function of the time delay $\kappa_1\tau$ and the two-photon loss rate κ_2/κ_1 for the driving strength $E_d/\kappa_1 = 0.1$. The inset show the cross section of the main plot along the lateral axis, i.e., the time-delay dependence of the second-order correlation function $g^{(2)}(\tau)$, with the five different values of the two-photon loss rate $\kappa_2/\kappa_1 = 0, 0.1, 0.5, 1, \text{ and } 5$.

In Fig. 4(a), we display the calculated phonon emission spectra $S(\omega)$ as a function of the frequency ω for seven different values of the two-photon loss κ_2 . As can be seen, the phonon emission spectra possess a symmetrical single-peak structure, which is of typical Lorentzian shape reminiscent of a weakly driven two-level system [107]. The peak values are located at $\omega = \omega_d$, indicating synchronization to the external driving. Here it is worth

pointing out that, without the nonlinear two-photon loss and only with the linear single-phonon loss corresponding to the case of $\kappa_2/\kappa_1 = 0$ in Fig. 4(a), the spectral line is flat and the phonon emission output is almost equal to zero. This is due to the fact that the applied driving field is considerably weak, $E_d = 0.1\kappa_1$ in this linear oscillator system. When E_d is comparable to κ_1 , the phonon emission output, with a Lorentzian shape and a linewidth given by κ_1 , can occur (not shown). With increasing κ_2 , the amount of phonon emission is enhanced distinctly owing to the presence and raise of the nonlinearity. Correspondingly, the spectral width of the emission is increased. For gradually increasing κ_2 from a zero value, the steady-state occupations of all Fock states (including $|1\rangle$) decrease since there is an additional relaxation channel opened, as is also confirmed by Eqs. (16) and (17) or Eqs. (31) and (32). Therefore, with increasing the κ_2/κ_1 ratio we can expect an increasing spectral width and emission amplitude.

In Fig. 4(b), we plot the amount of phonon emission $S(\omega = \omega_a)$ on the vdP oscillator resonance with the driving (i.e., $\Delta = 0$) as a function of κ_2 (left scale). $S(\omega = \omega_a)$ rises up quickly with κ_2 . For the sake of direct comparison with the above emission amount, again we show the second-order correlation function $g^{(2)}(0)$ in Fig. 4(b) (right scale). It is evident from these plots that the changes of $S(\omega = \omega_a)$ are opposite to $g^{(2)}(0)$; strong phonon antibunching is accompanied by the high amount of phonon emission, which is beneficial to the $g^{(2)}(0)$ measurement in practical experiments. For the sake of clarity, we depict contour plot of $S(\omega)$ as a function of ω and κ_2 in Fig. 4(c), the cuts of which through the horizontal axis correspond to Fig. 4(a). In a word, the stronger the antibunching is, the higher the collected fluorescence (the power spectral density) is, as expected.

For all the discussions above, so far we only con-

sider the zero-time-delay second-order correlation function $g^{(2)}(0)$. Now we focus on $g^{(2)}(\tau)$ with time delay τ . Figure 5 depicts the behavior of $g^{(2)}(\tau)$ as a function of both the time delay τ and the two-phonon loss κ_2 in a 2D contour plot. The inset in the main plot intuitively displays $g^{(2)}(\tau)$ versus τ for various values of κ_2 shown in the legend. Note that, the delayed $g^{(2)}(\tau)$ is only computed for $\tau \geq 0$, because it is formally symmetric about $\tau = 0$, i.e., $g^{(2)}(-\tau) = g^{(2)}(\tau)$ as mentioned before. We see from these figures that $g^{(2)}(\tau)$ monotonically increases from a value smaller than 1 (indicating antibunched phonon emission) to 1 (indicating coherent phonon emission) with τ for a given nonzero value of κ_2 . In particular, for $\kappa_2 = 0$, $g^{(2)}(\tau)$ is identically equal to 1. For a sufficient τ , $g^{(2)}(\tau)$ reaches the value of 1. Most obviously, a minimum value of $g^{(2)}(\tau)$ is obtained at $\tau = 0$. The minimum value of $g^{(2)}(\tau)$ diminishes with increasing κ_2 . Also, $g^{(2)}(\tau)$ persists at some value below unity over a long time, on the order of $1/\kappa_1$. From another point of view, it is found from Fig. 5 that the relationship $g^{(2)}(\tau) > g^{(2)}(0)$ is always satisfied for $\kappa_2 \neq 0$, which violates the Cauchy-Schwarz inequality $g^{(2)}(\tau) \leq g^{(2)}(0)$ related to classical light and thus shows the phenomenon of phonon antibunching or sub-Poissonian statistics related to nonclassical light [107–110].

VI. FEASIBILITY OF EXPERIMENTALLY IMPLEMENTING A QUANTUM VDP OSCILLATOR

Regarding the experimental feasibility of our scheme, we note that two typical setups, (i) an ion trap [91–97] and (ii) an optomechanical membrane [104–106], have demonstrated the possibility of implementing a vdP oscillator. First, for the ion trap setup proposed originally in Refs. [91, 92], the oscillator mode \hat{a} in Eq. (1) stands for a linearly damped motional degree of freedom of the trapped ion. Correspondingly, the linear one-phonon damping can occur when the standard laser cooling techniques are utilized [104]. One can engineer the nonlinear damping via applying sideband transitions to remove energy quanta, for example, the two-phonon loss can be carried out by laser exciting a harmonically trapped ion to its red motional sideband by removing two phonons at a time [91, 92]. In this scenario, the one- and two-phonon loss rates are both of the order of kHz, with $\kappa_2 \geq \kappa_1$ [91–93, 96, 97]. As also shown in Refs. [91, 97], it is possible to resolve sidebands and suppress off-resonant excitations for several tens of low-energy modes.

Second, for the optomechanical “membrane-in-the-middle” system [105, 106, 113] or the mechanical self-oscillation in cavity optomechanical system [114–116], one can take into account a moderate quality factor membrane with the linear mechanical damping. The nonlinear two-phonon damping can be implemented by exploiting a laser red-detuned with two mechanical frequencies relative to the two-phonon sideband. One can apply an

electric field gradient created near the membrane to create the driving force.

As a side note, the present phonon mode can be extended to a stationary photonic mode in an optical system, such as a microwave resonator or an optical cavity. Strong two-photon loss can also be realized successfully through the Josephson junction in superconducting circuit with high tunability [112] or through using an on-chip toroidal microcavity immersed in rubidium vapor [86].

Finally, one can use the objective to collect the phonon or photon emission from the oscillator mode \hat{a} . Then it is sent to a Hanbury-Brown–Twiss (HBT) configuration, consisting of a 50 : 50 beam splitter and a pair of single-phonon or single-photon counting detectors. The normalized second-order correlation function of interest, characterizing the quantum statistics of particle sources, can be measured by this HBT setup (see, for instance, Refs. [107–109], and references therein). Thus, we expect that an experimental implementation of our scheme is feasible in the present state of the art.

VII. CONCLUSIONS

In summary, we have introduced an alternative route towards highly nonclassical phonon emission statistics in a driven quantum vdP oscillator subject to both the linear one-phonon and nonlinear two-phonon damping by evaluating the second-order correlation function $g^{(2)}$ numerically and analytically. With experimentally achievable parameters, strong antibunching in the emitted phonon statistics is revealed by the full numerical simulations using a quantum master equation, which is in good agreement with analytical calculations utilizing a three-vdP-oscillator-level model by assuming that only the three lowest Fock states of the vdP oscillator have non-negligible occupations under weak driving. It is shown that the degree of phonon antibunching is limited by the rate of the two-phonon loss in this vdP oscillator, and the antibunching is enhanced considerably with growing the two-phonon loss. So, the two-phonon loss is very important for the realization of a good single-phonon device. The degree of phonon antibunching can be kept high even when $\kappa_2 < \kappa_1$. Suitable conditions for strong phonon antibunching generation and single-phonon emission are identified in the parameter regimes. On the other hand, we also numerically calculate the fluorescence phonon emission spectra $S(\omega)$, given by the power spectral density of the driven vdP oscillator. We further find that high phonon emission amplitudes, simultaneously accompanied by strong phonon antibunching, can be obtained, which are beneficial to the HBT measurement of the emitted phonons in practical experiments. Lastly, following the original proposals in Refs. [91, 92], we illustrate specific implementations applying a harmonically trapped ion and an optomechanical membrane in the middle. Our model’s description of

the interplay between one-phonon and two-phonon losses and their effects is not limited to phononic systems and should be generally applicable to photonic systems. This vdP architecture provides a feasible way of realizing efficient single-phonon or single-photon sources for quantum information processing tasks.

ACKNOWLEDGEMENTS

We are grateful to Rong Yu's help in improving this manuscript. The present research is supported in part

by the National Natural Science Foundation of China (NSFC) through Grant No. 11675058 and by the National Key Research and Development Program of China under Contract No. 2016YFA0301200.

-
- [1] N. Gisin and R. Thew, Quantum communication, *Nat. Photon.* **1**, 165–171 (2007).
- [2] H. J. Kimble, The quantum internet, *Nature (London)* **453**, 1023–1030 (2008).
- [3] J. L. O'Brien, A. Furusawa, and J. Vučković, Photonic quantum technologies, *Nat. Photon.* **3**, 687–695 (2009).
- [4] I. Buluta and F. Nori, Quantum simulators, *Science* **326**, 108–111 (2009).
- [5] C. H. Bennett and D. P. DiVincenzo, Quantum information and computation, *Nature (London)* **404**, 247–256 (2000).
- [6] V. Giovannetti, S. Lloyd, and L. Maccone, Advances in quantum metrology, *Nat. Photon.* **5**, 222–229 (2011).
- [7] I. Aharonovich, D. Englund, and M. Toth, Solid-state single-photon emitters, *Nat. Photon.* **10**, 631–641 (2016).
- [8] J. McKeever, A. Boca, A. D. Boozer, R. Miller, J. R. Buck, A. Kuzmich, and H. J. Kimble, Deterministic generation of single photons from one atom trapped in a cavity, *Science* **303**, 1992–1994 (2004).
- [9] T. Wilk, S. C. Webster, A. Kuhn, and G. Rempe, Single-atom single-photon quantum interface, *Science* **317**, 488–490 (2007).
- [10] O. Gazzano, S. Michaelis de Vasconcellos, C. Arnold, A. Nowak, E. Galopin, I. Sagnes, L. Lanco, A. Lemaître, and P. Senellart, Bright solid-state sources of indistinguishable single photons, *Nat. Commun.* **4**, 1425 (2013).
- [11] L. D. Santis, C. Antón, B. Reznichenko, N. Somaschi, G. Coppola, J. Senellart, C. Gómez, A. Lemaître, I. Sagnes, A. G. White, L. Lanco, A. Auffèves, and P. Senellart, A solid-state single-photon filter, *Nat. Nanotechnol.* **12**, 663–667 (2017).
- [12] Y.-M. He, Y. He, Y.-J. Wei, D. Wu, M. Atatüre, C. Schneider, S. Höfling, M. Kamp, C.-Y. Lu, and J.-W. Pan, On-demand semiconductor single-photon source with near-unity indistinguishability, *Nat. Nanotechnol.* **8**, 213–217 (2013).
- [13] F.-Y. Hong and S.-J. Xiong, Single-photon transistor using microtoroidal resonators, *Phys. Rev. A* **78**, 013812 (2008).
- [14] T. Volz, A. Reinhard, M. Winger, A. Badolato, K. J. Hennessy, E. L. Hu, and A. Imamoglu, Ultrafast all-optical switching by single photons, *Nat. Photon.* **6**, 605–609 (2012).
- [15] A. Babazadeh, M. Erhard, F. Wang, M. Malik, R. Nouroozi, M. Krenn, and A. Zeilinger, High-Dimensional Single-Photon Quantum Gates: Concepts and Experiments, *Phys. Rev. Lett.* **119**, 180510 (2017).
- [16] B. Dayan, A. S. Parkins, T. Aoki, E. P. Ostby, K. J. Vahala, and H. J. Kimble, A Photon Turnstile Dynamically Regulated by One Atom, *Science* **319**, 1062–1065 (2008).
- [17] R. Huang, A. Miranowicz, J.-Q. Liao, F. Nori, and H. Jing, Nonreciprocal Photon Blockade, *Phys. Rev. Lett.* **121**, 153601 (2018).
- [18] I. Carusotto and C. Ciuti, Quantum fluids of light, *Rev. Mod. Phys.* **85**, 299–366 (2013).
- [19] H. J. Kimble, *in Cavity Quantum Electrodynamics*, edited by P. Berman (Academic, San Diego, 1994).
- [20] J. Vučković, *Quantum optics and cavity QED with quantum dots in photonic crystals*. In: *Quantum Optics and Nanophotonics*. Edited by: C. Fabre, V. Sandoghdar, N. Treps, and L. F. Cugliandolo (Oxford University Press, Oxford, 2017), pp. 365–406.
- [21] W. Leoński and R. Tanaś, Possibility of producing the one-photon state in a kicked cavity with a nonlinear Kerr medium, *Phys. Rev. A* **49**, R20–R23 (1994).
- [22] A. Imamoglu, H. Schmidt, G. Woods, and M. Deutsch, Strongly Interacting Photons in a Nonlinear Cavity, *Phys. Rev. Lett.* **79**, 1467–1470 (1997).
- [23] J. M. Fink, M. Göppl, M. Baur, R. Bianchetti, P. J. Leek, A. Blais, and A. Wallraff, Climbing the Jaynes-Cummings ladder and observing its \sqrt{n} nonlinearity in a cavity QED system. *Nature (London)* **454**, 315–318 (2008).
- [24] J. Kasprzak, S. Reitzenstein, E. A. Muljarov, C. Kistner, C. Schneider, M. Strauss, S. Höfling, A. Forchel, and W. Langbein, Up on the Jaynes-Cummings ladder of a quantum-dot/microcavity system, *Nat. Mater.* **9**, 304–308 (2010).
- [25] F. P. Laussy, E. del Valle, M. Schrapp, A. Laucht, and J. J. Finley, Climbing the Jaynes-Cummings ladder by photon counting, *J. Nanophoton.* **6**, 061803 (2012).
- [26] K. M. Birnbaum, A. Boca, R. Miller, A. D. Boozer, T. E. Northup, and H. J. Kimble, Photon blockade in an optical cavity with one trapped atom, *Nature (London)* **436**, 87–90 (2005).
- [27] K. Hennessy, A. Badolato, M. Winger, D. Gerace, M. Atatüre, S. Gulde, S. Fält, E. L. Hu, and A. Imamoglu, Quantum nature of a strongly coupled single quantum dot-cavity system, *Nature (London)* **445**, 896–899 (2007).

- [28] A. Faraon, I. Fushman, D. Englund, N. Stoltz, P. Petroff, and J. Vučković, Coherent generation of nonclassical light on a chip via photon-induced tunnelling and blockade, *Nat. Phys.* **4**, 859–863 (2008).
- [29] A. Reinhard, T. Volz, M. Winger, A. Badolato, K. J. Hennessy, E. L. Hu, and A. Imamoglu, Strongly correlated photons on a chip, *Nat. Photon.* **6**, 93–96 (2012).
- [30] K. Müller, A. Rundquist, K. A. Fischer, T. Sarmiento, K. G. Lagoudakis, Y. A. Kelaita, C. S. Muñoz, E. del Valle, F. P. Laussy, and J. Vučković, Coherent Generation of Nonclassical Light on Chip via Detuned Photon Blockade, *Phys. Rev. Lett.* **114**, 233601 (2015).
- [31] W.-W. Deng, G.-X. Li, and H. Qin, Enhancement of the two-photon blockade in a strong-coupling qubit-cavity system, *Phys. Rev. A* **91**, 043831 (2015).
- [32] C. Hamsen, K. N. Tolazzi, T. Wilk, and G. Rempe, Two-Photon Blockade in an Atom-Driven Cavity QED System, *Phys. Rev. Lett.* **118**, 133604 (2017).
- [33] M. Koch, C. Sames, M. Balbach, H. Chibani, A. Kubanek, K. Murr, T. Wilk, and G. Rempe, Three-Photon Correlations in a Strongly Driven Atom-Cavity System, *Phys. Rev. Lett.* **107**, 023601 (2011).
- [34] M. Radulaski, K. A. Fischer, and J. Vučković, *Nonclassical Light Generation From III-V and Group-IV Solid-State Cavity Quantum Systems*, in *Advances in Atomic, Molecular, and Optical Physics* (Academic Press, New York, 2017), Vol. 66, pp. 111–179.
- [35] E. Illes and S. Hughes, Photon antibunching in strongly coupled exciton-semiconductor cavity systems: Role of off-resonant coupling to multiple excitons, *Phys. Rev. B* **81**, 121310(R) (2010).
- [36] M. Bradford and J.-T. Shen, Architecture dependence of photon antibunching in cavity quantum electrodynamics, *Phys. Rev. A* **92**, 023810 (2015).
- [37] C. Lang, D. Bozyigit, C. Eichler, L. Steffen, J. M. Fink, A. A. Abdumalikov, M. Baur, S. Filipp, M. P. da Silva, A. Blais, and A. Wallraff, Observation of Resonant Photon Blockade at Microwave Frequencies Using Correlation Function Measurements, *Phys. Rev. Lett.* **106**, 243601 (2011).
- [38] A. J. Hoffman, S. J. Srinivasan, S. Schmidt, L. Spietz, J. Aumentado, H. E. Türeci, and A. A. Houck, Dispersive Photon Blockade in a Superconducting Circuit, *Phys. Rev. Lett.* **107**, 053602 (2011).
- [39] Y.-x. Liu, X. W. Xu, A. Miranowicz, and F. Nori, From blockade to transparency: Controllable photon transmission through a circuit-QED system, *Phys. Rev. A* **89**, 043818 (2014).
- [40] J. T. Shen and S. H. Fan, Strongly Correlated Two-Photon Transport in a One-Dimensional Waveguide Coupled to a Two-Level System, *Phys. Rev. Lett.* **98**, 153003 (2007).
- [41] J. T. Shen and S. H. Fan, Strongly correlated multiparticle transport in one dimension through a quantum impurity, *Phys. Rev. A* **76**, 062709 (2007).
- [42] T. Shi and S. Fan, Two-photon transport through a waveguide coupling to a whispering-gallery resonator containing an atom and photon-blockade effect, *Phys. Rev. A* **87**, 063818 (2013).
- [43] M. Arcari, I. Söllner, A. Javadi, S. Lindskov Hansen, S. Mahmoodian, J. Liu, H. Thyrrestrup, E. H. Lee, J. D. Song, S. Stobbe, and P. Lodahl, Near-Unity Coupling Efficiency of a Quantum Emitter to a Photonic Crystal Waveguide, *Phys. Rev. Lett.* **113**, 093603 (2014).
- [44] D. S. Wild, E. Shahmoon, S. F. Yelin, and M. D. Lukin, Quantum Nonlinear Optics in Atomically Thin Materials, *Phys. Rev. Lett.* **121**, 123606 (2018).
- [45] P. Rabl, Photon Blockade Effect in Optomechanical Systems, *Phys. Rev. Lett.* **107**, 063601 (2011).
- [46] M. Aspelmeyer, T. J. Kippenberg, and F. Marquardt, Cavity optomechanics, *Rev. Mod. Phys.* **86**, 1391–1452 (2014).
- [47] J. Restrepo, I. Favero, and C. Ciuti, Fully coupled hybrid cavity optomechanics: Quantum interferences and correlations, *Phys. Rev. A* **95**, 023832 (2017).
- [48] L. Neumeier, T. E. Northup, and D. E. Chang, Reaching the optomechanical strong-coupling regime with a single atom in a cavity, *Phys. Rev. A* **97**, 063857 (2018).
- [49] Y. H. Zhou, H. Z. Shen, X. Y. Zhang, and X. X. Yi, Zero eigenvalues of a photon blockade induced by a non-Hermitian Hamiltonian with a gain cavity, *Phys. Rev. A* **97**, 043819 (2018).
- [50] B. Li, R. Huang, X.-W. Xu, A. Miranowicz, and H. Jing, Nonreciprocal unconventional photon blockade in a spinning optomechanical system, *Photon. Res.* **7**, 630–641 (2019).
- [51] D. E. Chang, V. Vuletić, and M. D. Lukin, Quantum nonlinear optics—photon by photon, *Nat. Photon.* **8**, 685–694 (2014).
- [52] M. Gullans, D. E. Chang, F. H. L. Koppens, F. J. García de Abajo, and M. D. Lukin, Single-Photon Nonlinear Optics with Graphene Plasmons, *Phys. Rev. Lett.* **111**, 247401 (2013).
- [53] R. Sáez-Blázquez, J. Feist, A. I. Fernández-Domínguez, and F. J. García-Vidal, Enhancing photon correlations through plasmonic strong coupling, *Optica* **4**, 1363–1367 (2017).
- [54] F. Peyskens and D. Englund, Quantum photonics model for nonclassical light generation using integrated nanoplasmonic cavity-emitter systems, *Phys. Rev. A* **97**, 063844 (2018).
- [55] A. Majumdar, C. M. Dodson, T. K. Fryett, A. Zhan, S. Buckley, and D. Gerace, Hybrid 2D material nanophotonics: A scalable platform for low-power nonlinear and quantum optics, *ACS Photon.* **2**, 1160–1166 (2015);
- [56] A. Ryou, D. Rosser, A. Saxena, T. Fryett, and A. Majumdar, Strong photon antibunching in weakly nonlinear two-dimensional exciton-polaritons, *Phys. Rev. B* **97**, 235307 (2018).
- [57] T. Ramos, V. Sudhir, K. Stannigel, P. Zoller, and T. J. Kippenberg, Nonlinear Quantum Optomechanics via Individual Intrinsic Two-Level Defects, *Phys. Rev. Lett.* **110**, 193602 (2013).
- [58] A. Miranowicz, M. Paprzycka, Y.-x. Liu, J. Bajer, and F. Nori, Two-photon and three-photon blockades in driven nonlinear systems, *Phys. Rev. A* **87**, 023809 (2013).
- [59] D. Yu, Single-photon emitter based on an ensemble of lattice-trapped interacting atoms, *Phys. Rev. A* **89**, 063809 (2014).
- [60] J. Leppäkangas, M. Fogelström, A. Grimm, M. Hofheinz, M. Marthaler, and G. Johansson, Antibunched Photons from Inelastic Cooper-Pair Tunneling, *Phys. Rev. Lett.* **115**, 027004 (2015).
- [61] C. J. Zhu, Y. P. Yang, and G. S. Agarwal, Collective multiphoton blockade in cavity quantum electrodynamics, *Phys. Rev. A* **95**, 063842 (2017).

- [62] T. C. H. Liew and V. Savona, Single photons from coupled quantum modes, *Phys. Rev. Lett.* **104**, 183601 (2010).
- [63] M.-A. Lemonde, N. Didier, and A. A. Clerk, Antibunching and unconventional photon blockade with Gaussian squeezed states, *Phys. Rev. A* **90**, 063824 (2014).
- [64] M. Bamba, A. Imamoglu, I. Carusotto, and C. Ciuti, Origin of strong photon antibunching in weakly nonlinear photonic molecules, *Phys. Rev. A* **83**, 021802(R) (2011).
- [65] A. Majumdar, M. Bajcsy, A. Rundquist, and J. Vučković, Loss-enabled sub-Poissonian light generation in a bimodal nanocavity, *Phys. Rev. Lett.* **108**, 183601 (2012).
- [66] Y. L. Liu, G. Z. Wang, Y.-x. Liu, and F. Nori, Mode coupling and photon antibunching in a bimodal cavity containing a dipole quantum emitter, *Phys. Rev. A* **93**, 013856 (2016).
- [67] J. Li and Y. Wu, Quality of photon antibunching in two cavity-waveguide arrangements on a chip, *Phys. Rev. A* **98**, 053801 (2018).
- [68] C. Wang, Y.-L. Liu, R. Wu, and Y.-x. Liu, Phase-modulated photon antibunching in a two-level system coupled to two cavities, *Phys. Rev. A* **96**, 013818 (2017).
- [69] A. Majumdar and D. Gerace, Single-photon blockade in doubly resonant nanocavities with second-order nonlinearity, *Phys. Rev. B* **87**, 235319 (2013).
- [70] H. Flayac and V. Savona, Input-output theory of the unconventional photon blockade, *Phys. Rev. A* **88**, 033836 (2013).
- [71] S. Ferretti, V. Savona, and D. Gerace, Optimal antibunching in passive photonic devices based on coupled nonlinear resonators, *New J. Phys.* **15**, 025012 (2013).
- [72] D. Gerace and V. Savona, Unconventional photon blockade in doubly resonant microcavities with second-order nonlinearity, *Phys. Rev. A* **89**, 031803(R) (2014).
- [73] H. Flayac, D. Gerace, and V. Savona, An all-silicon single-photon source by unconventional photon blockade, *Sci. Rep.* **5**, 11223 (2015).
- [74] H. Flayac and V. Savona, Unconventional Photon Blockade, *Phys. Rev. A* **96**, 053810 (2017).
- [75] X.-W. Xu and Y. Li, Tunable photon statistics in weakly nonlinear photonic molecules, *Phys. Rev. A* **90**, 043822 (2014).
- [76] H. Z. Shen, Y. H. Zhou, and X. X. Yi, Tunable photon blockade in coupled semiconductor cavities, *Phys. Rev. A* **91**, 063808 (2015);
- [77] Y. H. Zhou, H. Z. Shen, and X. X. Yi, Unconventional photon blockade with second-order nonlinearity, *Phys. Rev. A* **92**, 023838 (2015).
- [78] H. Flayac and V. Savona, Single photons from dissipation in coupled cavities, *Phys. Rev. A* **94**, 013815 (2016).
- [79] V. Savona, Unconventional photon blockade in coupled optomechanical systems, arXiv:1302.5937.
- [80] X. W. Xu and Y. J. Li, Antibunching photons in a cavity coupled to an optomechanical system, *J. Phys. B: At. Mol. Phys.* **46**, 035502 (2013).
- [81] A. Miranowicz, J. Bajer, N. Lambert, Y.-x. Liu, and F. Nori, Tunable multiphonon blockade in coupled nanomechanical resonators, *Phys. Rev. A* **93**, 013808 (2016).
- [82] B. Sarma and A. K. Sarma, Unconventional photon blockade in three-mode optomechanics, *Phys. Rev. A* **98**, 013826 (2018).
- [83] M. Bamba and C. Ciuti, Counter-polarized single-photon generation from the auxiliary cavity of a weakly nonlinear photonic molecule, *Appl. Phys. Lett.* **99**, 171111 (2011).
- [84] O. Kyriienko, I. A. Shelykh, and T. C. H. Liew, Tunable single-photon emission from dipolaritons, *Phys. Rev. A* **90**, 033807 (2014).
- [85] J. C. López Carreño, C. Sánchez Muñoz, D. Sanvitto, E. del Valle, and F. P. Laussy, Exciting Polaritons with Quantum Light, *Phys. Rev. Lett.* **115**, 196402 (2015).
- [86] Y.-P. Huang and P. Kumar, Antibunched Emission of Photon Pairs via Quantum Zeno Blockade, *Phys. Rev. Lett.* **108**, 030502 (2012).
- [87] J. H. Li, C. L. Ding, and Y. Wu, Enhanced photon antibunching via interference effects in a configuration, *Phys. Rev. A* **100**, 033814 (2019).
- [88] H. J. Snijders, J. A. Frey, J. Norman, H. Flayac, V. Savona, A. C. Gossard, J. E. Bowers, M. P. van Exter, D. Bouwmeester, and W. Löffler, Observation of the Unconventional Photon Blockade, *Phys. Rev. Lett.* **121**, 043601 (2018).
- [89] C. Vaneph, A. Morvan, G. Aiello, M. Féchant, M. Aprili, J. Gabelli, and J. Estève, Observation of the Unconventional Photon Blockade Effect in the Microwave Domain, *Phys. Rev. Lett.* **121**, 043602 (2018).
- [90] B. van der Pol, LXXXVIII. On “relaxation-oscillations,” *Philos. Mag.* **2**, 978–992 (1926).
- [91] T. E. Lee and H. R. Sadeghpour, Quantum Synchronization of Quantum van der Pol Oscillators with Trapped Ions, *Phys. Rev. Lett.* **111**, 234101 (2013).
- [92] S. Walter, A. Nunnenkamp, and C. Bruder, Quantum Synchronization of a Driven Self-Sustained Oscillator, *Phys. Rev. Lett.* **112**, 094102 (2014).
- [93] N. Lörch, E. Amitai, A. Nunnenkamp, and C. Bruder, Genuine Quantum Signatures in Synchronization of Anharmonic Self-Oscillators, *Phys. Rev. Lett.* **117**, 073601 (2016).
- [94] C. Navarrete-Benlloch, T. Weiss, S. Walter, and G. J. de Valcárcel, General Linearized Theory of Quantum Fluctuations around Arbitrary Limit Cycles, *Phys. Rev. Lett.* **119**, 133601 (2017).
- [95] T. Weiss, S. Walter, and F. Marquardt, Quantum-coherent phase oscillations in synchronization, *Phys. Rev. A* **95**, 041802(R) (2017).
- [96] S. Sonar, M. Hajdušek, M. Mukherjee, R. Fazio, V. Vedral, S. Vinjanampathy, and L.-C. Kwek, Squeezing Enhances Quantum Synchronization, *Phys. Rev. Lett.* **120**, 163601 (2018).
- [97] S. Dutta and N. R. Cooper, Critical Response of a Quantum van der Pol Oscillator, *Phys. Rev. Lett.* **123**, 250401 (2019).
- [98] T. Weiß, Nonlinear dynamics in quantum synchronization and topological transport, Dissertation, 2017. <https://opus4.kobv.de/opus4-fau/files/8704/TalithaWeissDissertation.pdf>
- [99] E. Amitai, Phase and amplitude dynamics of quantum self-oscillators, Dissertation, 2018. <https://edoc.unibas.ch/64965/1/Dissertation>
- [100] T. E. Lee, C.-K. Chan, and S. Wang, Entanglement tongue and quantum synchronization of disordered oscillators, *Phys. Rev. E* **89**, 022913 (2014).
- [101] S. Walter, A. Nunnenkamp, and C. Bruder, Quantum synchronization of two Van der Pol oscillators, *Ann. Phys. (Berlin)* **527**, 131–138 (2015).

- [102] E. Amitai, M. Koppenhöfer, N. Lörch, and C. Bruder, Quantum effects in amplitude death of coupled anharmonic self-oscillators, *Phys. Rev. E* **97**, 052203 (2018).
- [103] M. R. Jessop, W. Li, and A. D. Armour, Phase synchronization in coupled bistable oscillators, arXiv:1906.07603v2 [quant-ph].
- [104] J. I. Cirac, R. Blatt, P. Zoller, and W. D. Phillips, Laser cooling of trapped ions in a standing wave, *Phys. Rev. A* **46**, 2668–2681 (1992).
- [105] A. Jayich, J. Sankey, B. Zwickl, C. Yang, J. Thompson, S. Girvin, A. Clerk, F. Marquardt, and J. Harris, Dispersive optomechanics: a membrane inside a cavity, *New J. Phys.* **10**, 095008 (2008).
- [106] J. D. Thompson, B. M. Zwickl, A. M. Jayich, F. Marquardt, S. M. Girvin, and J. G. E. Harris, Strong dispersive coupling of a high-finesse cavity to a micromechanical membrane, *Nature (London)* **452**, 72–75 (2008).
- [107] M. O. Scully and M. S. Zubairy, *Quantum Optics* (Cambridge University Press, Cambridge, 1997).
- [108] C. Gardiner and P. Zoller, *Quantum Noise: A Handbook of Markovian and Non-Markovian Quantum Stochastic Methods with Applications to Quantum Optics* (Springer, Berlin, 2004).
- [109] G. S. Agarwal, *Quantum Optics* (Cambridge University Press, Cambridge, 2013).
- [110] H.-P. Breuer and F. Petruccione, *The Theory of Open Quantum Systems* (Oxford University Press, Oxford, 2002).
- [111] J. Gallego, W. Alt, T. Macha, M. Martinez-Dorantes, D. Pandey, and D. Meschede, Strong Purcell Effect on a Neutral Atom Trapped in an Open Fiber Cavity, *Phys. Rev. Lett.* **121**, 173603 (2018).
- [112] Z. Leghtas, S. Touzard, I. M. Pop, A. Kou, B. Vlastakis, A. Petrenko, K. M. Sliwa, A. Narla, S. Shankar, M. J. Hatridge, M. Reagor, L. Frunzio, R. J. Schoelkopf, M. Mirrahimi, and M. H. Devoret, Confining the state of light to a quantum manifold by engineered two-photon loss, *Science* **347**, 853–857 (2015).
- [113] A. Nunnenkamp, K. Børkje, J. G. E. Harris, and S. M. Girvin, Cooling and squeezing via quadratic optomechanical coupling, *Phys. Rev. A* **82**, 021806(R) (2010).
- [114] F. Marquardt, J. G. E. Harris, and S. M. Girvin, Dynamical multistability induced by radiation pressure in high-finesse micromechanical optical cavities, *Phys. Rev. Lett.* **96**, 103901 (2006).
- [115] T. J. Kippenberg, H. Rokhsari, T. Carmon, A. Scherer, and K. J. Vahala, Analysis of radiation-pressure induced mechanical oscillation of an optical microcavity, *Phys. Rev. Lett.* **95**, 033901 (2005).
- [116] C. Metzger, M. Ludwig, C. Neuenhahn, A. Ortlieb, I. Favero, K. Karrai, and F. Marquardt, Self-induced oscillations in an optomechanical system driven by bolometric backaction, *Phys. Rev. Lett.* **101**, 133903 (2008).